An Investigation of Bifurcation Acoustic Treatment Effects on Aft-Fan Engine Nacelle Noise

Douglas M. Nark* and Michael G. Jones†
NASA Langley Research Center, Hampton, VA 23681-2199, U.S.A

Increasing air traffic and more stringent aircraft noise regulations continue to expand requirements on aircraft noise reduction capabilities for conventional and unconventional aircraft configurations. A major component of the overall aircraft noise is the sound associated with the propulsion system mounted in the engine nacelle. Acoustic liners mounted in the aircraft engine nacelles provide a significant portion of the current fan noise reduction. However, they must be further optimized if challenging noise reduction goals are to be achieved. One area within the aft bypass duct that may be an excellent candidate for increased attention is the acoustic treatment on the engine bifurcations (i.e., engine pylon and lower bifurcation). This paper describes a fundamental study of the effects of bifurcation treatment on simulated aft fan noise, as well as the validation of numerical tools to predict such effects. Five bifurcation configurations (four treated and one hardwall) were fabricated and tested in the NASA Langley Curved Duct Test Rig. Results show that mode scattering may occur due to both the presence of the bifurcation, as well as variable impedance distributions on the bifurcation surface. Future work will also include optimization of bifurcation treatments for testing in the Curved Duct Test Rig. These initial results are promising and this work provides valuable information for further study and improvement of the performance of bifurcation acoustic treatments.

I. Introduction

Increasing air traffic and more stringent aircraft noise regulations continue to expand requirements on aircraft noise reduction capabilities for conventional and unconventional aircraft configurations. A major component of the overall aircraft noise is the sound associated with the propulsion system mounted in the engine nacelle. In addition, the utilization of advanced fan designs (including higher bypass ratios) and shorter engine nacelles has highlighted a need for increased reduction of this noise component over a broad frequency range. Acoustic liners mounted in the aircraft engine nacelles provide a significant portion of the current fan noise reduction. However, they must be further optimized if challenging noise reduction goals are to be achieved. Thus, there is significant interest in the development and optimal placement of advanced broadband acoustic liner concepts. One area within the aft bypass duct that may be an excellent candidate for increased attention is the acoustic treatment on the engine bifurcations (i.e., engine pylon and lower bifurcation).

This paper describes a fundamental study of the effects of bifurcation treatment on simulated aft fan noise, as well as the validation of numerical tools to predict such effects. The test facility and associated measurements are described in Section II. The liner modeling and computational approach are then presented in more detail in Sections III and IV. Evaluation of measured data and comparison with predictions are provided in Section V. Finally, concluding remarks regarding some of the more significant results and further areas of interest are presented in Section VI.

II. Test Facility and Acoustic Measurements

A. Flow Duct

The NASA Langley Curved Duct Test Rig (CDTR) was chosen for the experimental portion of this study. The facility is designed to assess the acoustic and aerodynamic performance of aircraft engine nacelle liners with a test section ranging between 100% and 25% of the scale of business jet or large passenger jet aircraft engine bypass ducts, respectively. These attributes, as well as the overall measurement capabilities, make it ideal for the fundamental experimental investigation of the effects of bifurcation treatment involved in this study.

*Senior Research Scientist, Structural Acoustics Branch, Research Directorate, AIAA Associate Fellow
†Senior Research Scientist, Structural Acoustics Branch, Research Directorate, AIAA Associate Fellow

The CDTR (see Figure 1) is an open loop wind tunnel that uses a fan to draw unconditioned atmospheric air through the 6 in. (15.24 cm) wide by 15 in. (38.10 cm) high test section. Sound is generated using an array of loudspeakers to achieve a maximum sound level on the order of 140 dB. The incident sound can be tonal or broadband. For tone noise, the magnitude and phase of the voltage signal to each loudspeaker is controlled such that a selected mode can be generated in the duct and undesired modes are suppressed. A subset of the upstream microphone array is used as the control to adjust the signals to the loudspeakers. In this study, tones are generated at 130 dB from 400 to 3000 Hz in 200 Hz increments at centerline Mach numbers of 0.0, 0.25, and 0.45. Sound is generated to produce individual cut-on duct modes up to the (3,0) mode, where (v,h) refer to the mode number in the vertical and horizontal directions, respectively. The control system design ensures that the sound incident on the test section is predominantly composed of the selected mode and is at least 10 dB greater than any other mode in the duct. The recorded signals from the upstream and downstream microphone arrays are analyzed to determine the mode distribution upstream and downstream of the test section. Additional details on the data analysis, as well as general CDTR operation may be found in previous papers.[1–3]

B. Bifurcation Configurations

An NACA 0012-64 airfoil, with a chord length of 12 in. (30.48 cm) and span of 6 in. (15.24 cm), was used as the profile for all bifurcation configurations in this study. The full test matrix consists of five bifurcations fabricated via additive manufacturing: one hardwall and four treated configurations. As seen in the computational model in Figure 3, the bifurcation was mounted chordwise parallel to flow in the CDTR, at the midpoint of the 15 in. dimension, such that it split the CDTR test section into two equal sections. The treated configurations, which are shown in Figure 4, include acoustic treatment (consisting of perforated facsheets over open chambers) that begins approximately 2.3 in. (6.03 cm) from the leading edge and extends 6.4 in. (16.26 cm) over the upper and/or lower surface of the bifurcation. In this figure, the portions of the bifurcation through which fluid (and therefore sound) may flow are identified with red lines. To clarify this point further, a photo of configuration 1 showing the top surface of the bifurcation is provided in Figure 5. Here, the 0.3 in. x 0.3 in. (0.762 cm x 0.762 cm) cells with 0.05 in. x 0.05 in. (0.127 cm x 0.127 cm) shoulders that form the liner core are clearly visible. Thus, the treated area is comprised of 15 spanwise cells and 16 chordwise cells. The facesheet, if present, is included within the printed part and is comprised of 18 circular holes per cell with diameter of 0.033 in. (0.083 cm). Thus, if open, a given 0.3 in. x 0.3 in. cell has a percent open area (POA) of 17.1%[a]. As seen in Figure 4, the treated configurations employ a variety of cell configurations to achieve different impedances. Configuration 1 includes open cells only on the top surface of the bifurcation and is indicative of a conventional liner configuration. Configuration 2 employs the same approach as configuration 1, except that the open cells alternate between the upper and lower surfaces in the chordwise direction such that there is effectively treatment on both surfaces. Configuration 3 employs a slotted core and therefore allows communication between adjacent cells in the chordwise direction. It should be noted that individual cells are always isolated in the spanwise direction and, therefore, this communication between adjacent cells occurs only in the chordwise direction. Finally, configuration 4 also employs a slotted core and differs from configuration 3 in that the open "channels" alternate between the upper and lower surface.

III. Impedance Modeling

In order to perform propagation predictions, the impedance of the treated configurations is required to apply the proper boundary condition on the bifurcation surface. The impedance prediction model used in this study combines two models presented in an earlier paper.[4] The first is a transmission line model[5] that assumes acoustic wave propagation through each layer of the liner and the second is a lumped element model[6–8] used to compute the impedance change across perforates. The normalized surface impedance spectra presented by each chamber of the liner are computed separately, and are then combined to determine an effective surface impedance spectrum that is assumed uniform across the liner surface.

To test the impedance modeling approach, a series of normal incidence tests was performed on configurations 1 and 3 in the NASA Langley normal incidence impedance tube (NIT).[9] As the NIT requires 2 in. x 2 in. (5.08 cm x 5.08 cm) samples, portions of the full bifurcation sample were taped to isolate specific areas for testing. Additional flat samples were fabricated via additive manufacturing for comparison with the in situ results. The leading edge of configuration 1 was first considered as illustrated in Figure 6. Here, the test region of the full bifurcation is indicated by the white region in Figure 6a. A side view of the flat NIT sample built to mimic the test portion of the in situ

[a]Note that the resultant smeared porosity will therefore be substantially lower and will be different for the various configurations

sample is then shown in Figure 6b. Finally, the predicted and measured (for both samples) normalized resistance and reactance are presented in Figures 6c and 6d. In this case, the predicted and measured reactance values match very well. However, there is some discrepancy with the in situ resistance component. This is believed to be caused by the difficulties in performing normal incidence testing on a curved sample. This appears to be confirmed by the significantly improved match between the predicted and measured flat sample resistance.

It should be noted that these impedance values represent the effective smeared impedance produced by the combination of various cells. In subsequent propagation predictions, the impedance presented by the individual cells were used. However, this testing still provides important verification of the input impedance, as the individual cell impedance values are required to correctly predict the smeared impedance. Two additional locations on configuration 1 were tested and the results are presented in Figures 7 and 8. The results are similar to the first case and indicate that the impedance model is working well for the conventional configurations (at least with zero mean flow).

In contrast to configuration 1, configuration 3 incorporates a slotted core and therefore entails some additional modeling effort. The liner model requires a cell depth to be provided as input. In the case of configuration 1, this is a straightforward task. However, with the slotted core found in configuration 3, a decision must be made as to what constitutes the channel depth. In the initial modeling, the input depth was taken to be the centerline distance from the back of the facesheet to the backplate. This is illustrated by the dashed white line in the first channel of the slotted core example in Figure 9. For configuration 3, the in situ and flat NIT samples represented different chordwise sections and are therefore presented separately. The predicted and measured impedances for an interior portion of the full bifurcation are shown in Figure 10. While the resonant frequency appears to be fairly well captured, the frequency for antiresonance is not. The discrepancy is apparent in both the resistance and reactance curves. To alleviate possible sample curvature effects, a flat sample representing the leading edge portion of configuration 3 was subsequently tested in the NIT and the results are presented in Figure 11. The difference in the measured values obtained for the two configuration 3 samples may be explained by the depth change (i.e., different chordwise locations). However, the frequency for antiresonance is again underpredicted.

To further investigate the difficulties in predicting the slotted core impedance, a representative configuration 3 sample (see Figure 12) was fabricated using additive manufacturing for testing in the NASA Langley Grazing Flow Impedance Tube (GFIT).[10] At 2 inches (5.08 cm) wide and 8 inches (20.32 cm) long, the GFIT sample included the full chordwise extent of configuration 3 with 5 cells in the spanwise direction. Comparison of the predicted and educed impedances are presented in Figure 13 with results similar to those found with the NIT samples. In the presence of mean flow, the situation remains as seen in the results at $M = 0.25$ and 0.45 in Figures 14 and 15. As seen in these figures, the mass reactance decreases with Mach number and therefore antiresonance occurs at higher frequencies. This trend is captured by the prediction, but the frequency at which this occurs continues to be underpredicted.

Subsequent slotted core testing suggests that the partition height, h, (see Figure 9) has a large influence on impedance and proper modeling warrants further investigation. Therefore, rather than relying on an ad hoc adjustment of the input depth for these configurations, propagation predictions were limited to configurations 1 and 2. Future work will include slotted core configurations after further consideration of the associated impedance modeling.

IV. Duct Propagation Prediction

For the current investigation, duct propagation predictions were conducted using the CDUCT-LaRC (CDL) code over the computational domain presented in Figure 3. This code calculates the propagation of a given acoustic source ahead of the fan face or aft of the exhaust guide vanes in the inlet or exhaust ducts, respectively. The three-dimensional duct may include acoustic treatment (possibly circumferentially and radially segmented) and incorporate struts/bifurcations. All of the modules that currently make up the CDL framework have been discussed previously.[11] However, this discussion will focus on the propagation module, as it is most pertinent to this investigation.

The duct propagation module is based on the CDUCT code developed by Dougherty[12,13] and extended by Lan.[14] This code utilizes a parabolic approximation to the convected Helmholtz equation and offers a computationally efficient model that accounts for the complexities of fully three-dimensional nacelle configurations. To provide for such prediction capability, the CDL code supports multiblock propagation calculations in which grid connectivity is determined and data are transferred from upstream to downstream blocks without user intervention.[11] The propagation module output includes the acoustic potential or pressure within the duct, which may be utilized by the radiation module for acoustic radiation calculations.

While CDL can accept arbitrary source specification (i.e., it is not a modal code), the acoustic source distribution for the current study is specified in terms of duct modes to model the experimental setup. As mentioned above, CDTR testing entailed specification of a source mode that was controlled by the CDTR control system to be at least

10 dB above any other mode incident on the test section. Subsequent analysis of the microphone array downstream of the test section provides the mode distribution downstream of the bifurcation and, therefore, a measurement of any resultant modal scattering. Predictions first involve source specification using information from the modal decomposition of the upstream microphone array data. The predicted sound field within the CDTR is then obtained and modal decomposition performed at axial locations matching those of the upstream and downstream measurement arrays. Comparison of downstream measured and predicted mode power levels then provides an assessment of the propagation code capabilities in predicting the mode scattering effects caused by the hardwall/treated bifurcation.

V. Results and Discussion

For reasons discussed in Section III, propagation predictions were limited to the hardwall sample and configurations 1 and 2. As typical bifurcation treatment applications involve mean flow, cases without mean flow ($M = 0.0$) were not considered for presentation. Nevertheless, the measured data set remained large and posed a challenge in downselecting cases to illustrate modal scattering due to 1) the presence of the bifurcation, and/or 2) the presence of variable impedance distributions on the bifurcation surface. Therefore, cases involving mean flow with interaction between the dominant source mode and bifurcation were of particular interest. With the bifurcation positioned on the CDTR centerline, this meant vertical mode shapes without nodes at the centerline location (i.e., even number vertical modes).

Based on the explanation above, the plane wave source was first considered and results for the three configurations at a frequency of 1600 Hz and $M = 0.25$ are presented in Figure 16. Here, the modal content is presented as a bar chart with the specified source (matching the source field measured in the CDTR) represented as a solid blue bar. The predicted and measured downstream modal content is represented as "cross-hatched" red and green bars, respectively. The downstream field will typically consist of energy that has been scattered from the specified source content into other modes, with a corresponding reduction in source levels. The degree of scattering and any other energy loss is expected to depend on the bifurcation treatment. So, for the hardwall configuration, it is expected that only mode scattering will occur with no energy loss. Conversely, the treated configurations are expected to produce different modal content with a corresponding frequency dependent attenuation. Thus, for all three configurations in Figure 13, the plane wave source is clearly visible above all other modes. For configuration 1, there is scattering of energy into the higher modes in both the predictions and measurements. However, the measured results show additional power in the (3,0) mode that is not present in the predictions. This is likely due to the fact that this mode is fairly close to cut-off which can cause difficulties with the parabolic approximation in CDL. Results for configuration 2 and the hardwall case compare quite well. It is interesting to note that both the predictions and measurements show different mode scattering for the different configurations. For example, configuration 1 shows (1,0) and (3,0) mode levels that are not present for configuration 2 or the hardwall bifurcation. Similarly, the hardwall configuration shows little scattering into higher order modes. As the source specification is the same for all configurations, it would appear that this behavior is due to the variation in surface impedance on the bifurcation surface.

To illustrate this further, results for a (2,0) mode source are presented in Figure 17. In this case, mode scattering is present for all configurations. The predictions capture the measured modal energy transfer with slightly higher levels in the plane wave source. This is not entirely unexpected, as the energy transfer is to lower-order modes that are handled more accurately by the parabolic approximation. As was the case with the plane wave source, the different impedance distributions lead to different mode scattering behavior for the three configurations.

Results showing similar behavior were obtained across the range of cases. In order to avoid redundancy, select cases covering alternate mode sources and flow speeds are presented for completeness. Regarding alternate source modes, Figure 18 provides results for configuration 1 with (1,0) and (1,1) mode sources at $M = 0.25$. These are similar to the previous cases with the modal energy transfer captured in the numerical results. For the (1,1) source mode, it is interesting to note that mode scattering to a lower order vertical mode occurs. However, except for small evidence of energy in the (1,0) mode in the measured data, the energy remains in a mode of the same horizontal mode order. The consistency in horizontal mode order is to be expected since the acoustic treatment does not change in the spanwise direction (i.e., there is no apparent physical mechanism for transfer). Finally, example predictions for a (2,0) source mode at the higher Mach number ($M = 0.45$) are presented in Figure 19. Except for the presence of the (1,0) mode in measured data for configuration 1, results are similar to previous cases. The configuration 2 results show a rich modal content that is consistent between predictions and measurements.

It should be noted that the treated cases presented do not demonstrate a large amount of overall attenuation for several reasons. First, the single-degree-of-freedom treatments achieve maximum attenuation over a very narrow frequency range. Second, the overall treatment area is relatively small with axial treatment length to duct height

ratios (L/H) of 0.2 and 0.4 for configurations 1 and 2, respectively. Finally, since the goal of this initial study was to investigate modal scattering effects and validate the modeling approach, no attempt was made to optimize the treated configurations for application in the CDTR. Although they are not presented, a number of predictions (at frequencies for which testing was not performed) showed attenuation levels on the order of 7-8 dB. Thus, with increased confidence in the numerical modeling, future work will include optimization of treatment for additional CDTR testing.

VI. Concluding Remarks

This paper describes a fundamental experimental study of the effects of bifurcation treatment on aft fan noise, as well as the validation of numerical tools to predict such effects. Five bifurcation configurations (four treated and one hardwall) were fabricated and tested in the CDTR. Predicted impedance values of the single degree-of-freedom configurations matched measured values well. However, impedance prediction for the slotted core configurations tended to underpredict the frequency for antiresonance and these configurations will be investigated further in future work. The propagation predictions captured the energy transfer well and generally matched measured values. Results show that mode scattering may occur due to both the presence of the bifurcation, as well as variable impedance distributions on the bifurcation surface. Future work will also include optimization of bifurcation treatments for the CDTR. These initial results are promising and this work provides valuable information for further study and improvement of the performance of bifurcation acoustic treatments.

Acknowledgments

This research was funded by the Advanced Air Transport Technology (AATT) Project of the NASA Advanced Air Vehicles Program (AAVP). The support of Martha Brown, Max Reid, and William Leath for the acquisition and processing of CDTR data is gratefully acknowledged. The authors would also like to thank Brian Howerton and Rob Andrews for their assistance in the fabrication of the bifurcation samples.

References

[1]Gerhold, C. H., Cabell, R. H., and Brown, M. C., "Development of an Experimental Rig for Investigation of Higher Order Modes in Ducts," AIAA Paper 2006-2637, 2006.

[2]Gerhold, C. G., Brown, M. C., Jones, M. G., and Howerton, B. M., "Report on Recent Upgrades to the Curved Duct Test Rig at NASA Langley Research Center," AIAA Paper 2011-2896, 2011.

[3]Gerhold, C. H., Brown, M. C., and Jones, M. G., "Segmented Liner to Control Mode Scattering," AIAA Paper 2013-2078, 2013.

[4]Jones, M. G., Howerton, B. M., and Ayle, E., "Evaluation of Parallel-Element, Variable-Impedance, Broadband Acoustic Liner Concepts," AIAA Paper 2012-2194, 2012.

[5]Parrott, T. L. and Jones, M. G., "Parallel-Element Liner Impedances for Improved Absorption of Broadband Sound in Ducts," *Noise Control Engineering Journal*, Vol. 43, No. 6, 1995, pp. 183–195.

[6]Motsinger, R. E. and Kraft, R. E., "Design and Performance of Duct Acoustic Treatment: Aeroacoustics of Flight Vehicles; Chapter 14, Vol. 2: Noise Control," NASA RP 1258, August 1991.

[7]Jones, M. G., Parrott, T. L., and Watson, W. R., "Uncertainty and Sensitivity Analyses of a Two- Parameter Impedance Prediction Model," AIAA Paper 2008-2928, 2008.

[8]Parrott, T. L. and Jones, M. G., "Assessment of NASA's Aircraft Noise Prediction Capability, Chapter 6: Uncertainty in Acoustic Liner Impedance Measurement and Prediction," NASA TP 2102-215653, July 2012.

[9]Jones, M. G. and Stiede, P. E., "Comparison of methods for determining specific acoustic impedance," *Journal of the Acoustical Society of America*, Vol. 101, No. 5, May 1997, pp. 2694–2704.

[10]Jones, M. G., Watson, W. R., Parrott, T. L., and Smith, C. D., "Design and Evaluation of Modifications to the NASA Langley Flow Impedance Tube," AIAA Paper 2004-2837, 2004.

[11]Nark, D. M., Farassat, F., Pope, D. S., and Vatsa, V., "The Development of the Ducted Fan Noise Propagation and Radiation Code CDUCT-LaRC," AIAA Paper 2003-3242, 2003.

[12]Dougherty, R. P., "A Wave-Splitting Technique for Nacelle Acoustic Propagation," AIAA Paper 97-1652, 1997.

[13]Dougherty, R. P., "A Parabolic Approximation for Flow Effects on Sound Propagation in Nonuniform, Softwall, Ducts," AIAA Paper 99-1822, 1999.

[14]Lan, J. H., "Turbofan Duct Propagation Model," NASA CR 2001-211245, 2001.

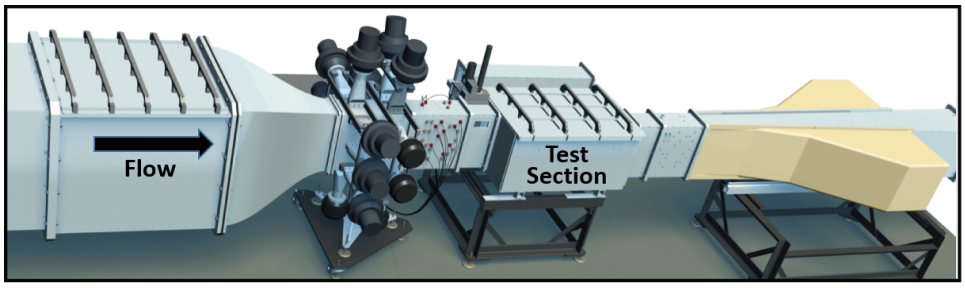

Figure 1: Artist rendering of the CDTR showing the flow condition section, acoustic drivers, and test section.

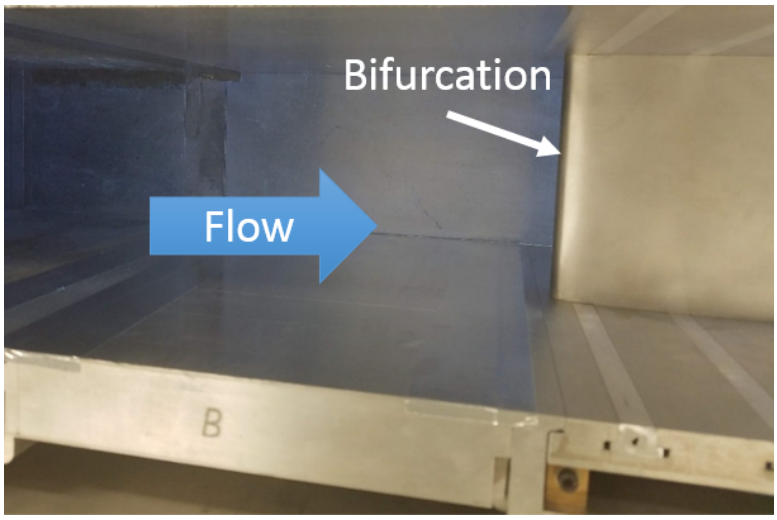

Figure 2: Top view of a hardwall bifurcation mounted in the CDTR.

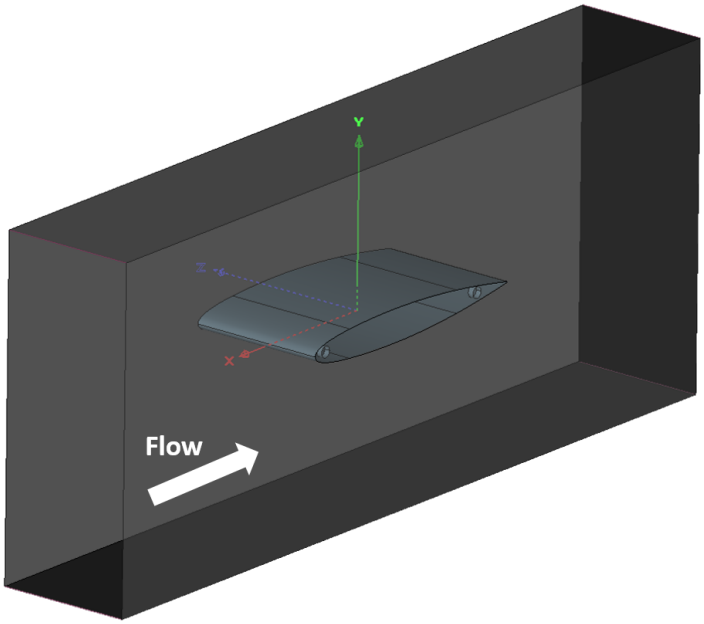

Figure 3: Model of the hardwall bifurcation in the CDTR test section.

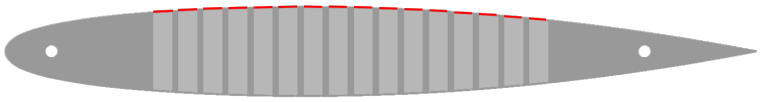

(a) Configuration 1.

(b) Configuration 2.

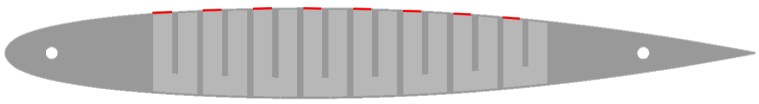

(c) Configuration 3.

(d) Configuration 4.

Figure 4: CDTR treated bifurcation sample configurations. Open facesheet areas are indicated in red.

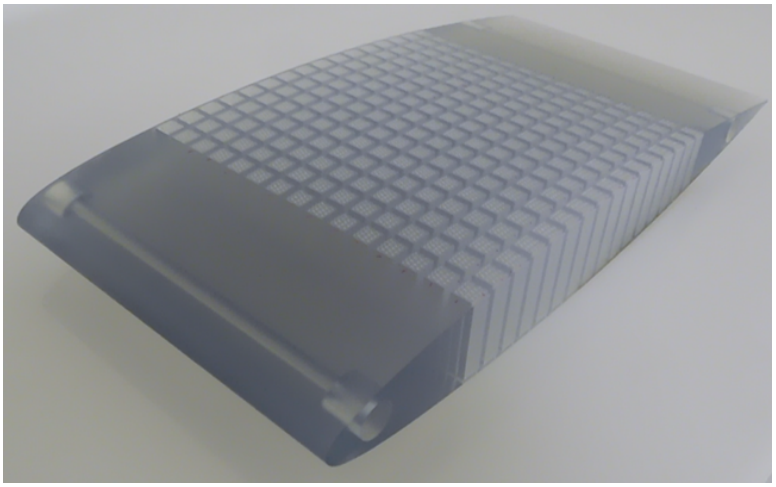

Figure 5: Top surface of the baseline bifurcation sample (configuration 1: single-degree of freedom) .

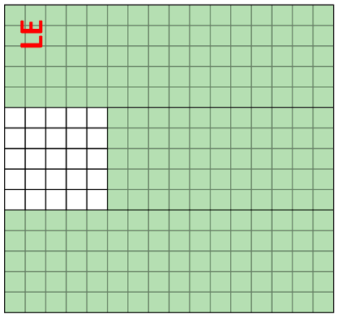

(a) NIT (in situ).

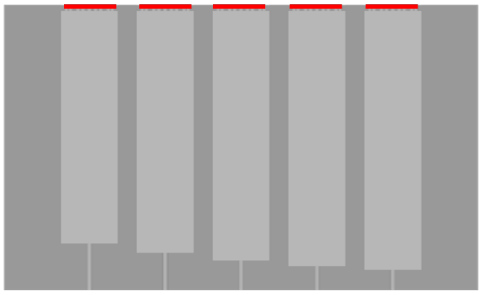

(b) NIT (2”x2”).

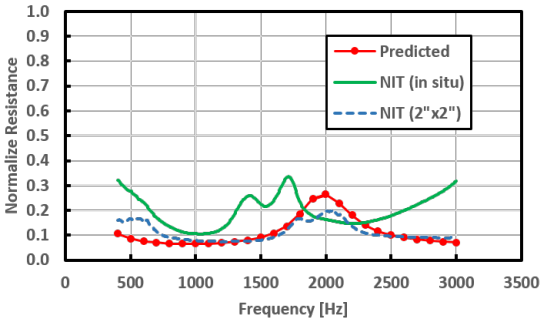

(c) Normalized Resistance.

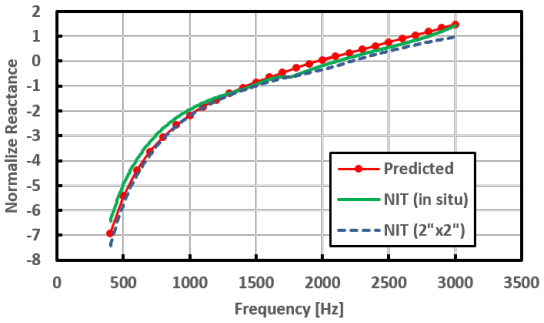

(d) Normalized Reactance.

Figure 6: Predicted and educed impedances for the leading edge portion of configuration 1 in the NIT.

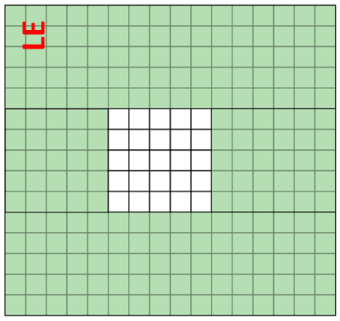

(a) NIT (in situ).

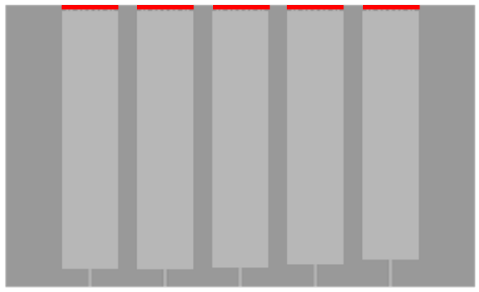

(b) NIT (2”x2”).

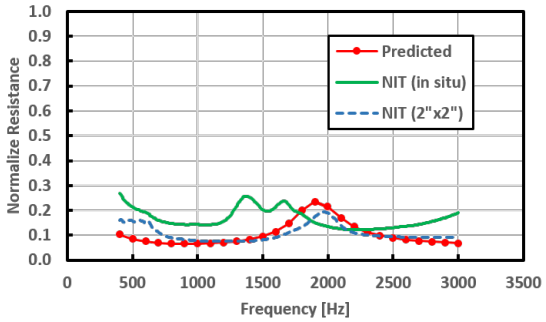

(c) Normalized Resistance.

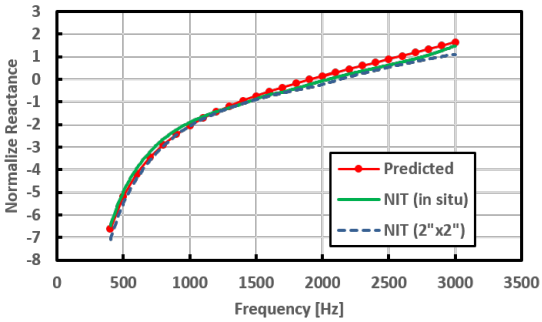

(d) Normalized Reactance.

Figure 7: Predicted and educed impedances for the center portion of configuration 1 in the NIT.

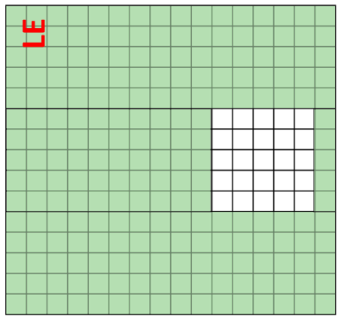

(a) NIT (in situ).

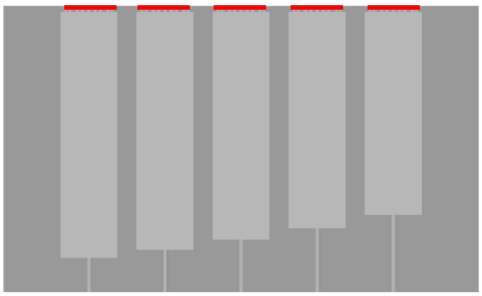

(b) NIT (2”x2”).

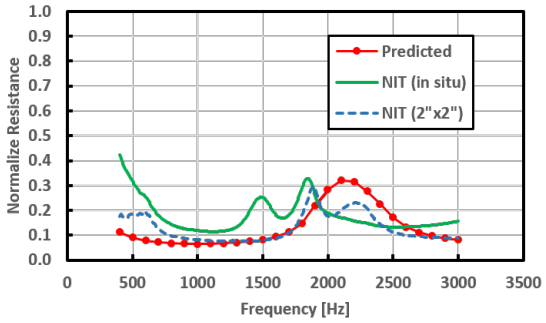

(c) Normalized Resistance.

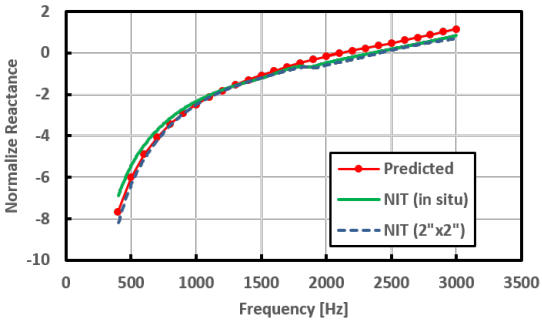

(d) Normalized Reactance.

Figure 8: Predicted and educed impedances for the trailing edge portion of configuration 1 in the NIT.

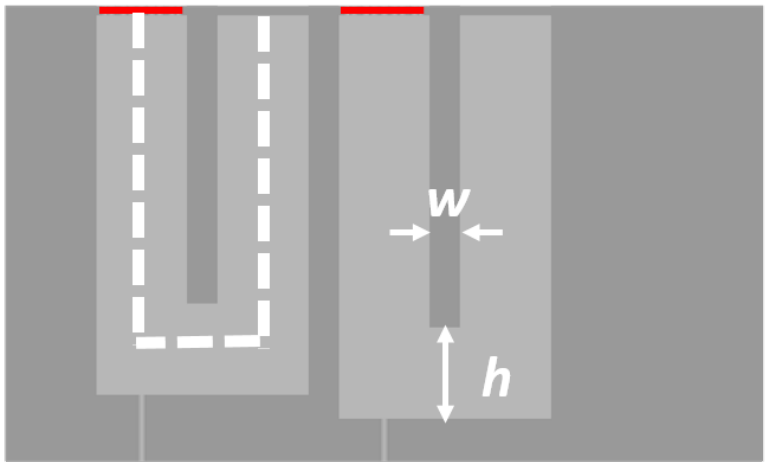

Figure 9: Slotted core example illustrating centerline channel depth assumption, as well as partition width, w, and height, h, variables.

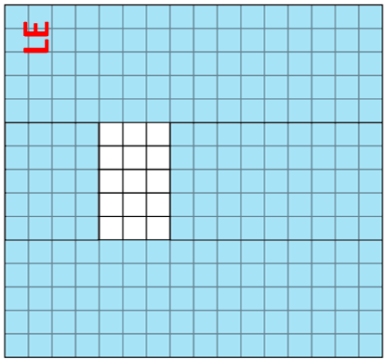

(a) NIT (in situ).

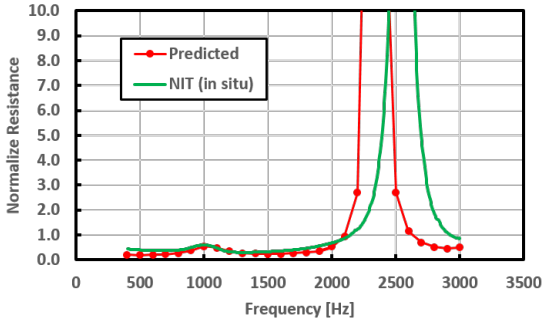

(b) Normalized Resistance.

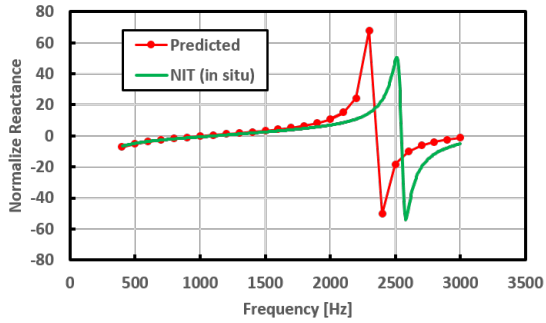

(c) Normalized Reactance.

Figure 10: Predicted and educed impedances for an interior portion of configuration 3 in the NIT.

(a) NIT (2"x2").

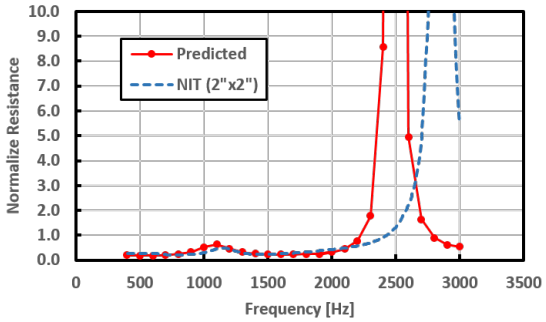

(b) Normalized Resistance.

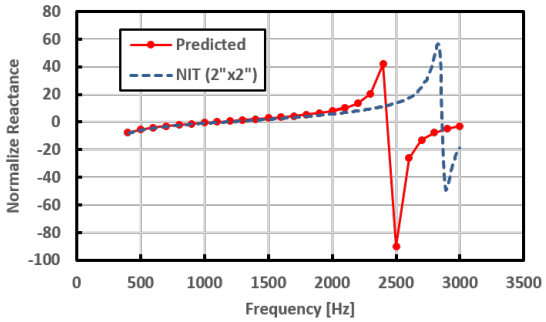

(c) Normalized Reactance.

Figure 11: Predicted and educed impedances for the leading edge portion of configuration 3 in the NIT.

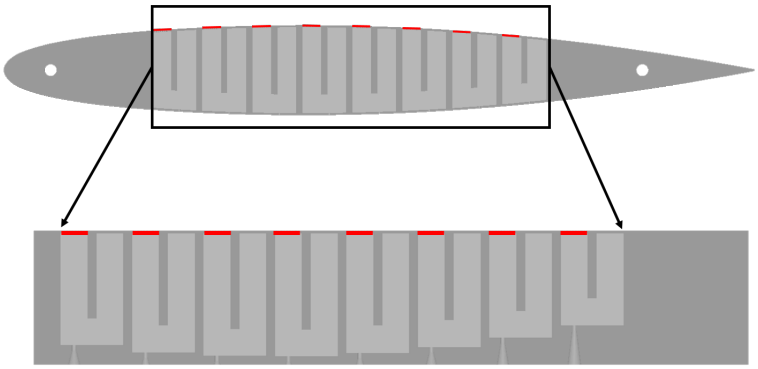

Figure 12: Flat GFIT sample replicating the slotted core of configuration 3.

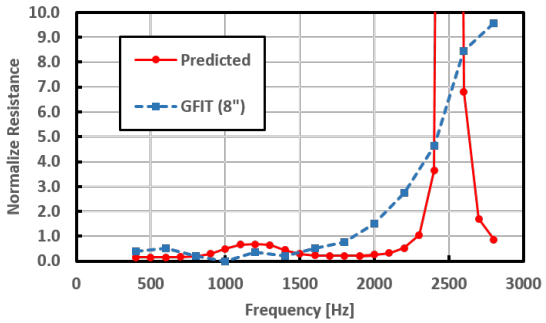

(a) Normalized Resistance.

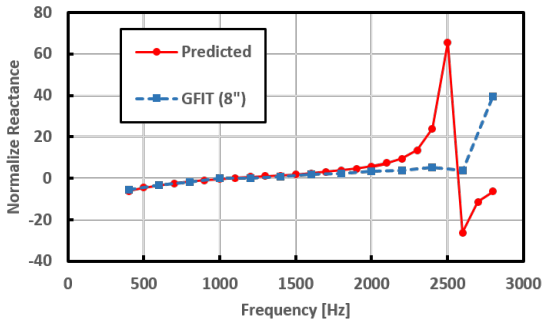

(b) Normalized Reactance.

Figure 13: Predicted and educed impedances for configuration BF3 in the GFIT ($M = 0.0$).

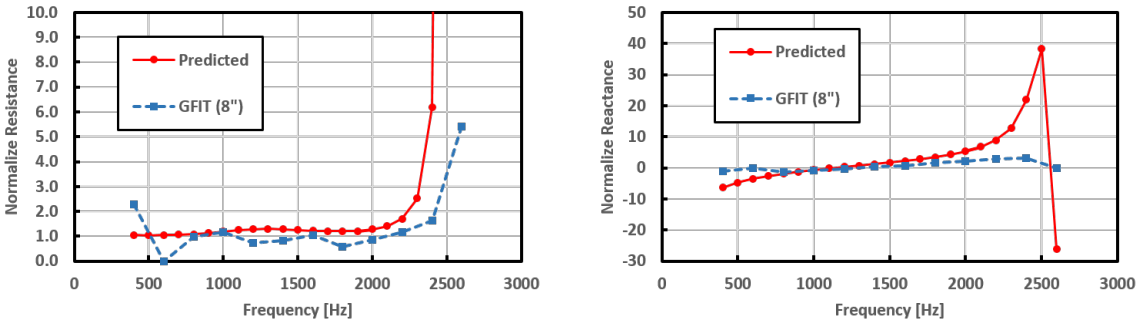

(a) Normalized Resistance.

(b) Normalized Reactance.

Figure 14: Predicted and educed impedances for configuration BF3 in the GFIT ($M = 0.25$).

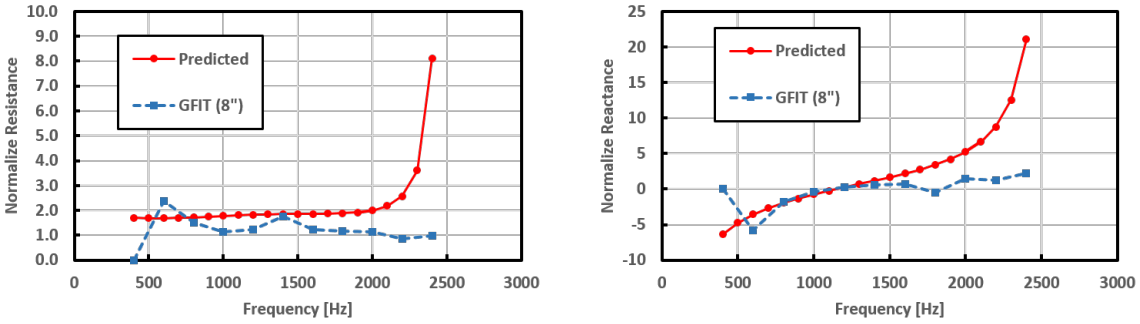

(a) Normalized Resistance.

(b) Normalized Reactance.

Figure 15: Predicted and educed impedances for configuration BF3 in the GFIT ($M = 0.45$).

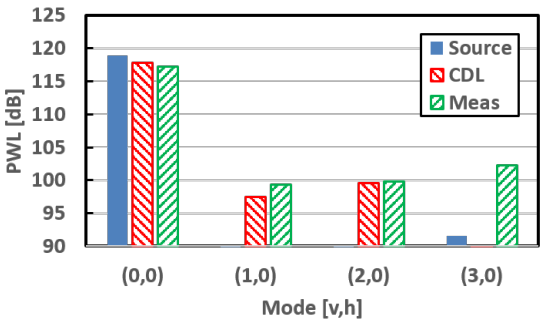

(a) Configuration 1

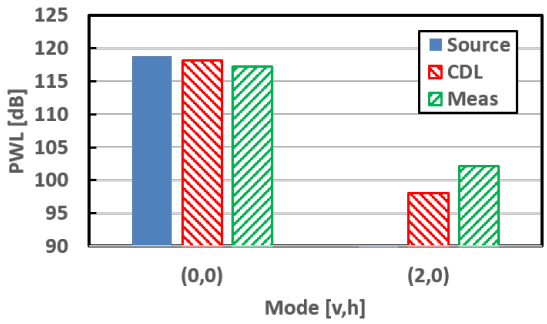

(b) Configuration 2

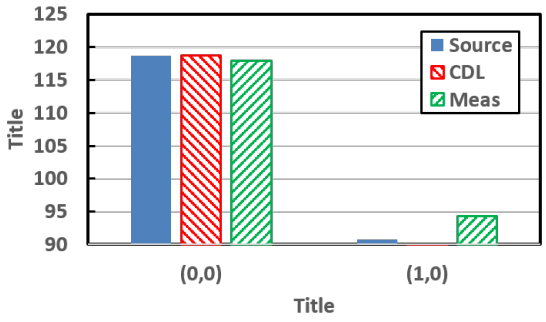

(c) Hardwall

Figure 16: Predicted and measured modal content for a plane wave (0,0) source at $f = 1600$ Hz and $M = 0.25$.

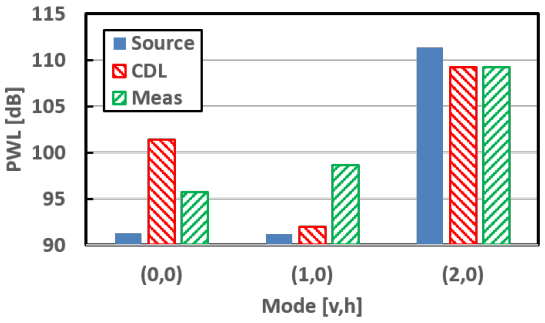

(a) Configuration 1

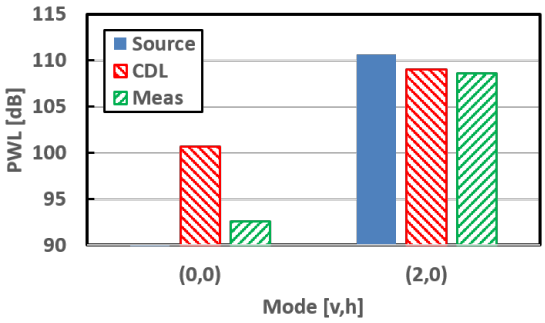

(b) Configuration 2

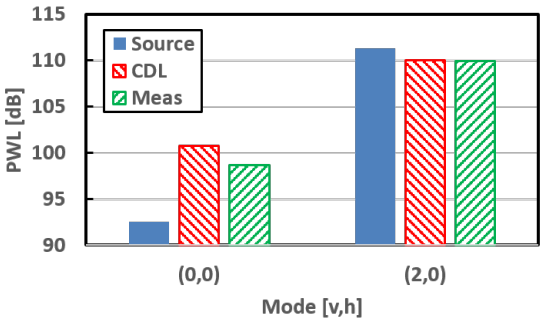

(c) Hardwall

Figure 17: Predicted and measured modal content for a mode (2,0) source at $f = 1200$ Hz and $M = 0.25$.

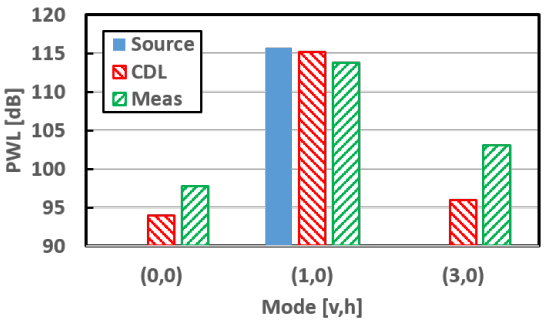

(a) Source mode: (1,0).

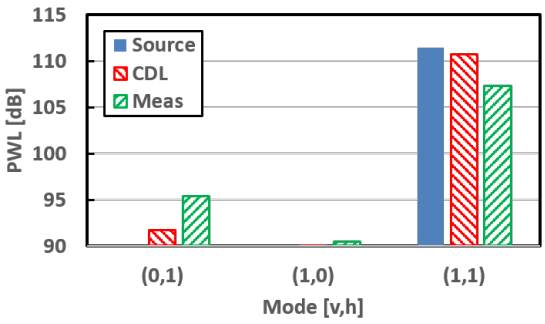

(b) Source mode: (1,1).

Figure 18: Predicted and measured modal content for configuration 1 with (1,0) and (1,1) modes source at $f = 1800$ Hz and $M = 0.25$.

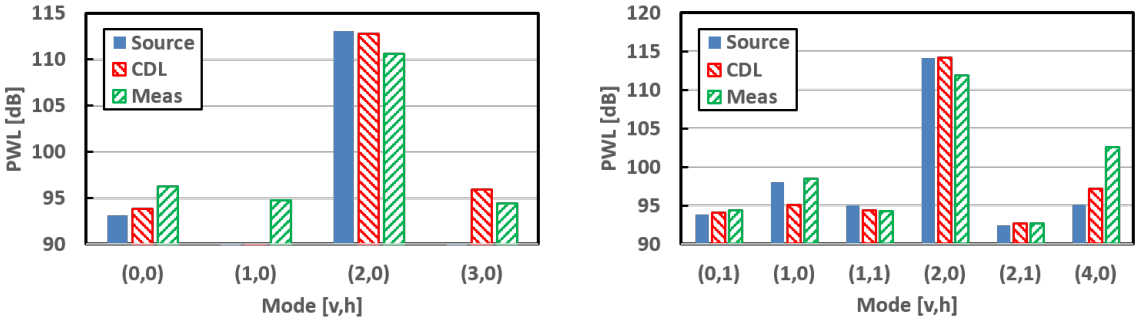

(a) Configuration 1 ($f = 2000$ Hz).

(b) Configuration 2 ($f = 2200$) Hz.

Figure 19: Predicted and measured modal content for a mode (2,0) source at $M = 0.45$.